

X-Ray Observations of the Sagittarius D H II Region toward the Galactic Center with Suzaku

Makoto SAWADA,¹ Masahiro TSUJIMOTO,^{2*} Katsuji KOYAMA,¹ Casey J. LAW,³
Takeshi Go TSURU,¹ and Yoshiaki HYODO¹

¹*Department of Physics, Graduate School of Science, Kyoto University
Kitashirakawa Oiwake-cho, Sakyo-ku, Kyoto 606-8502*

²*Department of Astronomy & Astrophysics, Pennsylvania State University
525 Davey Laboratory, University Park, PA 16802, USA*

³*Astronomical Institute “Anton Pannekoek”, University of Amsterdam
Kruislaan 403, 1098 SJ Amsterdam, The Netherlands
sawada@cr.scphys.kyoto-u.ac.jp*

(Received 2008 March 31; accepted)

Abstract

We present a Suzaku X-ray study of the Sagittarius D (Sgr D) H II region in the Galactic center region. Two $18' \times 18'$ images by the X-ray Imaging Spectrometer (XIS) encompass the entire Sgr D complex. Thanks to the low background, XIS discovered two diffuse sources with low surface brightness and obtained their high signal-to-noise ratio spectra. One is associated with the core of the Sgr D H II region, arising from the young stellar cluster. The other is a new object in the vicinity of the region. We also present 3.5 cm and 6.0 cm radio continuum maps of the new source using the 100 m Green Bank Telescope. We conclude that the source is a new supernova remnant (SNR; G1.2-0.0) based on: (1) the 0.9 ± 0.2 keV thermal X-ray spectrum with emission lines from highly ionized atoms; (2) the diffuse nature with an apparent extent of ~ 10 pc at the Galactic center distance inferred from the X-ray absorption ($\sim 8.5 \times 10^{22}$ cm⁻²); and (3) the nonthermal radio continuum spectral index (~ -0.5). Our discovery of an SNR in the Sgr D H II region leads to a revision of the view of this system, which had been considered to be a thermal H II region and its environment.

Key words: ISM: H II regions — ISM: individual (Sgr D) — ISM: supernova remnants — radio continuum: ISM — X-rays: ISM

1. Introduction

Sagittarius D (Sgr D) is one of the most intense radio sources in the Galactic center (GC) region known from the earliest days of GC radio observations (Downes & Maxwell 1966). It is composed of an H II region (Sgr D H II region or G1.13-0.10) and a supernova remnant (SNR; Sgr D SNR or G1.05-0.15) adjoining each other (figure 1a). Low-resolution radio continuum observations (Little 1974; Swarup et al. 1974; Downes et al. 1979) identified thermal emission from the H II region and nonthermal emission from the SNR.

The Sgr D H II region is associated with its natal giant molecular cloud (GMC), which has a velocity different from those typical of GMCs in the Galactic nuclear disk such as Sgr B2 (Lis 1991; Liszt 1992). In higher resolution radio continuum images (Mehringer et al. 1998; LaRosa et al. 2000; Yusef-Zadeh et al. 2004), the Sgr D H II region is comprised of several components of different spatial scales. Throughout this paper, we call the entire region “the Sgr D H II complex” and treat three components separately (figure 1a): (1) “core”, the brightest knot, which is referred to as “G1.12-0.10” (Liszt 1992; Mehringer et

al. 1998) or the “compact H II region” (Blum & Damiani 1999), (2) “extended”, a $\sim 7'$ shell surrounding the “core” (Blum & Damiani 1999), and (3) “tail”, the structure extending eastward from the “extended” component, which is labeled “G1.2+0.0” (Law et al. 2008). The “core” is an H II region with a Lyman continuum photon intensity equivalent of an O5.5 star based on its infrared properties (Odenwald & Fazio 1984; Blum & Damiani 1999). The latter two structures may be at the edge of the H II region; the “extended” component is created by ionizing photons from the “core” and the “tail” by gas escaping away from the “extended” component (Mehringer et al. 1998).

Recent observational results, however, are diverging away from this view of the Sgr D H II complex. There are two contradictory estimates of its distance. Narrow molecular line emission and broad H₂CO absorption features indicate that the complex is on the far side of the GC region (Mehringer et al. 1998), whereas the near-infrared star counts around the “core” suggest the system lies on the near side of the GC (Blum & Damiani 1999), possibly in the ~ 160 pc expanding molecular ring (Lis 1991). The latest radio continuum study on arcminute spatial scales indicates a mixture of thermal and nonthermal emission in this complex (Law et al. 2008), which historically had been considered solely a thermal radio source.

* Chandra Fellow

Table 1. Log of Suzaku and XMM-Newton observations.

Telescope/ Instrument	Sequence number	Field name	Aim point		Observation start date	Exposure time (ks)*
			α (J2000.0)	δ (J2000.0)		
Suzaku/XIS	501059010	north	17 ^h 48 ^m 22 ^s	-27°56'08"	2007/03/15	62.2/62.2
Suzaku/XIS	502020010	south	17 ^h 48 ^m 46 ^s	-28°08'00"	2007/09/06	139/139
XMM-Newton/EPIC	0112970101	obs00	17 ^h 48 ^m 44 ^s	-28°05'06"	2000/09/23	14.5/12.9
XMM-Newton/EPIC	0205240101	obs05	17 ^h 48 ^m 17 ^s	-28°07'50"	2005/02/26	28.7/16.6

* The exposure time after screening of XIS FI/BI for the Suzaku and EPIC MOS/pn for the XMM-Newton observations.

These new lines of evidence do not support the long-standing interpretation that the Sgr D H II complex is a single H II region and its environment. Rather, it is more likely that the system is made up of multiple components at various distances projected along the same line of sight. Previous results should be carefully reviewed and new observations should be conducted to better understand the system.

X-ray observations are indispensable in this pursuit. Both SNRs and GMCs can be identified through X-ray imaging as emission extended by ~ 10 pc. The two types of emission can be distinguished by their X-ray spectra; SNRs show thermal plasma with emission lines from highly ionized atoms (e.g., Becker et al. 1979), while GMCs show emission produced by external X-ray irradiation (Murakami et al. 2000). H II regions are also an emerging class of diffuse X-ray sources with a similar spatial scale. They show a variety of spectral shapes, including soft thermal (Townsend et al. 2003; Hyodo et al. 2008), hard thermal (Moffat et al. 2002; Ezoe et al. 2006), and nonthermal (Wolk et al. 2002; Law & Yusef-Zadeh 2004; Wang et al. 2006; Tsujimoto et al. 2007; Ezoe et al. 2006) emission. In addition to the X-ray emission, the measurement of the X-ray absorption gives a constraint on the distance and hence the physical scale of extended objects.

Several X-ray observations were reported in the Sgr D region. In a BeppoSAX study (Sidoli et al. 2001), diffuse X-ray emission was significantly detected from the Sgr D SNR and marginally detected from the Sgr D H II complex. In an ASCA study (Sakano et al. 2002), the image was plagued by stray lights from a nearby bright source and was unsuitable to search for diffuse X-ray sources. In an XMM-Newton study (Sidoli et al. 2006), dozens of point sources were identified, but no diffuse emission was detected presumably due to high background. The possible diffuse X-ray detection by BeppoSAX in the Sgr D H II complex has not been confirmed and no spectral information exists for this source.

We conducted X-ray observations of the Sgr D H II complex using the X-ray Imaging Spectrometer (XIS: Koyama et al. 2007a) onboard Suzaku (Mitsuda et al. 2007). The low background of XIS makes it particularly well-suited for finding diffuse sources of low surface brightness and yielding their high signal-to-noise ratio spectra. Indeed, a series of XIS studies in the GC region identified several new SNRs and irradiated GMCs (Koyama et al. 2007b; Mori et al. 2008; Nobukawa et al. 2008) and reported detailed spectroscopy of an H II region (Tsujimoto et al.

2007). Upon the confirmation of the previously claimed marginal diffuse detection in the Sgr D H II complex, we further aim to construct the X-ray spectrum which gives important insights into the origin of the emission and the entire complex.

Here, we present a significant detection of diffuse X-ray emission from the Sgr D H II complex with the Suzaku XIS. High signal-to-noise ratio spectra were obtained from two different diffuse sources. We discuss their X-ray characteristics and their association with sources observed in our study using the 100 m Green Bank Telescope (GBT) and in other archived multiwavelength data sets. Based on these data, we propose a new view of the Sgr D H II complex. In this paper, we supplement the Suzaku data with those taken by XMM-Newton in order to evaluate the contribution of point sources to the diffuse emission. Throughout this paper, we use east and west in the Galactic longitude direction, and north and south in the Galactic latitude direction for simplicity.

2. Observations

2.1. Suzaku

We used two XIS fields covering the Sgr D H II complex in the Suzaku GC mapping project (table 1). We hereafter call the two fields as north and south field (figure 1a). The north field covers the entire complex. The overlapping area of the north and south fields also cover a part of the complex, for which we additionally use the south field data. Results in the remaining part of the south field will be reported in a separate paper.

The XIS consists of four CCD cameras (XIS 0, 1, 2, and 3) each placed at the focal planes of the four X-ray Telescopes (XRT: Serlemitsos et al. 2007). One of the cameras (XIS 1) uses a back-illuminated (BI) CCD while the others (XIS 0, 2, and 3) use front-illuminated (FI) CCDs. One of the FIs (XIS 2) has not been functional since an unexpected anomaly in 2006 November.

The XIS is sensitive in an energy range of 0.2–12 keV with the FI CCDs superior in the hard band and the BI CCD in the soft band. For the purpose of mitigating the degradation of the energy resolution in the orbit, the XIS employs the spaced-row charge injection (SCI) technique (Bautz et al. 2004; Uchiyama et al. 2007). Artificial charges are periodically injected to fill charge traps caused by radiation damage in order to reduce the charge transfer inefficiency (CTI). In the present data, the resolution at 5.9 keV is measured to be ~ 150 eV (FI) and ~ 170 eV

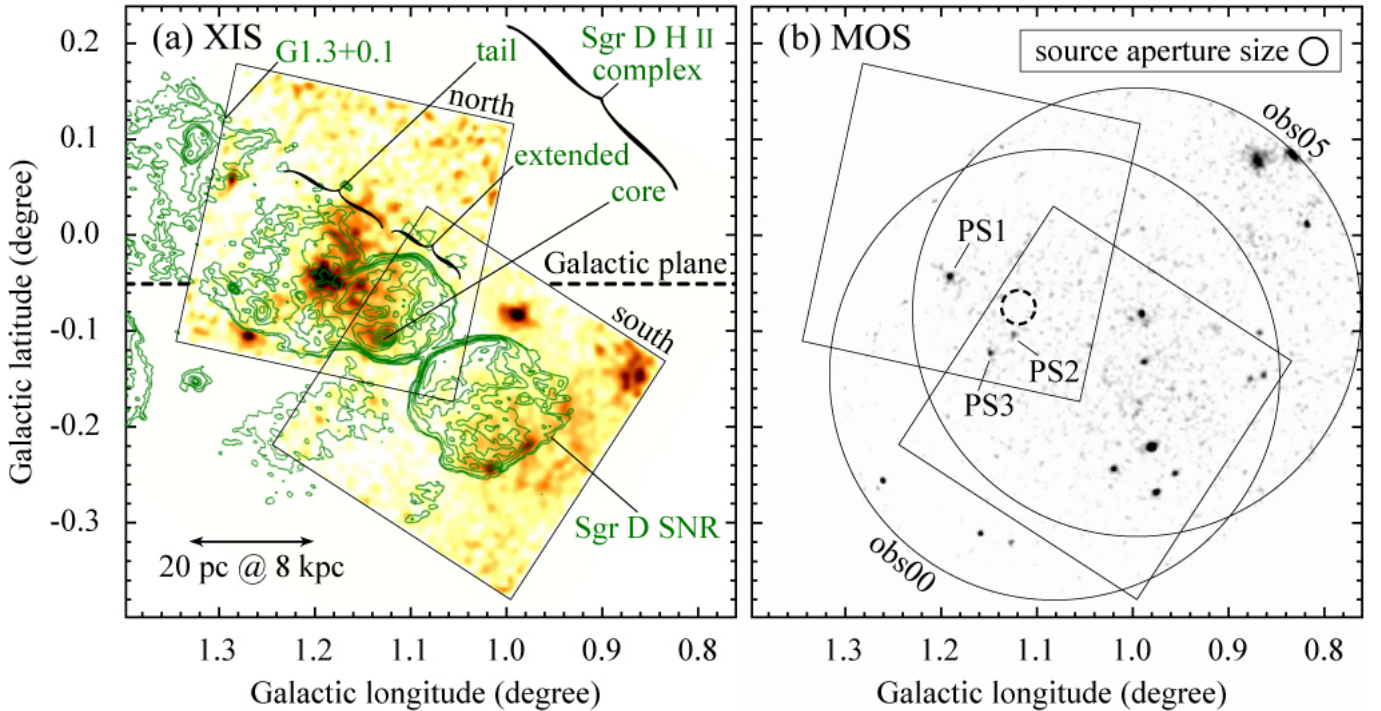


Fig. 1. Wide-band (0.7–5.5 keV) smoothed images by the (a) XIS and (b) MOS shown with the logarithmic intensity scale. Overlaid green contours in (a) are an 18 cm radio continuum map from the Very Large Array (VLA; Mehringer et al. 1998). The point source extraction aperture and background accumulation region are shown in (b). See § 3.2.1 for details. For the XIS image, we merged events with the three CCDs, subtracted the non-X-ray background (Tawa et al. 2008), corrected for the vignetting, and mosaicked the two fields with different exposure times normalized. The fields of view are shown with two solid squares with $18'$ in length. For the MOS image, we merged two CCDs and mosaicked the two fields with normalized exposures. The fields are shown with two circles with $30'$ in diameter.

(BI) in the full width at half maximum (FWHM) using the ^{55}Fe calibration sources installed in the two corners of each CCD.

Combined with the XRT, an $18' \times 18'$ region is covered with a pixel scale of $1'' \text{ pixel}^{-1}$. An angular resolution of $1'9$ – $2'3$ in the half power diameter (HPD) is almost independent of the off-axis angles within $\sim 10\%$. The total effective area excluding the inoperational XIS 2 is $\sim 430 \text{ cm}^2$ at 8 keV. Due to the Suzaku's low orbital altitude at $\sim 550 \text{ km}$, the XIS achieves a low and stable background environment suited for studying faint diffuse sources.

In the two observations presented here, the XIS was operated in the normal clocking mode with the SCI technique. Starting from the pipeline products in the processing version 2.0, we recalculated the energy scales by taking into account of the time dependence of the CTI and the positional dependence of the SCI efficiency.¹ The resultant systematic uncertainty in the energy gain is $\lesssim 10 \text{ eV}$ at 5.9 keV. We removed events during the South Atlantic Anomaly passages, Earth elevation angles below 5° , and

¹ See (http://heasarc.gsfc.nasa.gov/docs/suzaku/analysis/sci_gain_update.html) for details.

Earth day-time elevation angles below 20° . We also removed hot and flickering pixels. The net exposures are 62.2 and 139 ks for the north and south fields, respectively. We reduced the data using the software packages HEADAS² version 6.4 and XSpec (Arnaud 1996) version 11.3.2. In the spectral analysis, we used the redistribution matrix function released on 2006-02-13 and the auxiliary response function generated by a ray-tracing simulator (`xissimarfgen`; Ishisaki et al. 2007).

2.2. XMM-Newton

We retrieved the archived XMM-Newton (Jansen et al. 2001) data to supplement the Suzaku data, and found that two observations taken in 2000 and 2005 cover Sgr D. We hereafter refer to them as *obs00* and *obs05*, respectively (table 1). The *obs05* data were presented by Sidoli et al. (2006), upon which we add the *obs00* data to make deeper images. Both data sets were obtained with the European Photon Imaging Camera (EPIC), which is comprised of two MOS CCDs (Turner et al. 2001) and a pn CCD (Strüder et al. 2001).

The EPIC is sensitive in an energy range of 0.1–10 keV

² See (<http://heasarc.nasa.gov/lheasoft/>).

with an energy resolution of ~ 140 eV (MOS) and ~ 170 eV (pn) in the FWHM at 5.9 keV for the retrieved data. The MOS and pn cover a $\sim 30'$ diameter circle with a pixel scale of $1'' \text{ pixel}^{-1}$ and $4'' \text{ pixel}^{-1}$, respectively. The HPD and the total effective area at 8 keV are $4.''2\text{--}6.''6$ at the optical axis and $\sim 900 \text{ cm}^2$, respectively. The combination of XMM-Newton's large effective area and imaging capability makes EPIC observations highly sensitive to point sources.

In the two observations, both the MOS and the pn were operated in the full frame mode with the medium filter. We removed events taken during periods with background rates higher than $0.5 \text{ counts s}^{-1}$ (MOS) and $0.3 \text{ counts s}^{-1}$ (pn) in the 10–15 keV energy band. We also removed hot and flickering pixels. The resultant effective exposures are shown in table 1. The XMM-Newton Science Analysis System³ version 7.1.0 was used for reducing the EPIC data.

3. Results

3.1. Images

3.1.1. Wide-Band Images

Figure 1 shows the wide-band (0.7–5.5 keV) X-ray images obtained with the XIS and the EPIC MOS. Here, we restricted the energy range to be below 5.5 keV to eliminate the signals from the calibration sources in the XIS image. We find that the Sgr D H II complex is accompanied by both diffuse and point-like X-ray emission. The former is more noticeable in the XIS image while the latter is in the MOS image, reflecting the complementary capability of the two imagers.

In the MOS image (figure 1b), we found three bright point-like sources in and around the complex listed in the Second XMM-Newton Serendipitous Source Catalogue (Watson 2007): PS1 (2XMM J174835.9–275619), PS2 (2XMM J174841.1–280136), and PS3 (2XMM J174848.7–280100). We matched the astrometric positions between the XIS and the MOS images using bright and isolated point-like sources. The absolute astrometry of XMM-Newton is accurate to $\sim 2''^4$, while that of Suzaku can be uncertain up to $\sim 20''$ (Uchiyama et al. 2008). The XIS south field was shifted to match the MOS image by $(\Delta R. A., \Delta Dec.) = (0'', 22'')$, while the north field was unchanged as it is consistent with the MOS astrometric positions.

3.1.2. Band-Limited Images

XIS images were exposed for much longer times than MOS images (table 1). Sufficient photon counts enable us to construct both broad-band and narrow-band images with XIS. Figure 2 shows the close-up view of the Sgr D H II complex in four limited energy bands: (a) soft (0.7–2.0 keV), (b) medium (2.0–4.0 keV), (c) hard (4.0–5.5 keV), and (d) S XV $K\alpha$ (2.4–2.5 keV).

In the three broad-band images (figure 2a–2c), PS1 appears only in the soft and medium bands, indicating that

it is soft, lightly attenuated, and thus a foreground source. The soft band image lacks diffuse features. However, in the medium and hard bands, diffuse emission emerges with different colors at the north field center and at the Sgr D H II core. We consider that the two diffuse sources are different and call them DS1 and DS2 (figure 2).

In the narrow-band image tracing the S XV $K\alpha$ line emission (figure 2d), PS1 and DS1 are conspicuous. These sources are likely to be thermal emission of a few keV plasma temperatures. DS2, on the contrary, is faint in this band. This reinforces the claim that DS1 and DS2 have different origins.

3.2. Spectra

3.2.1. Point-Like Sources

We first present the spectral fits of the three bright point sources that may contaminate the diffuse emission. Figure 3 shows their background-subtracted spectra. For PS1, we used the XIS data as it is detected and the statistics is higher than the EPIC data. The source photons were accumulated from a $1'$ radius (the thick solid circle in figure 2a) to maximize the ratio against the background. The background photons were from a concentric annulus around the source (the thick dashed annulus) to suppress the contamination from DS1. In the spectrum (figure 3a), emission lines are seen from several species of highly ionized atoms. We fitted the data with a thin-thermal plasma model (*apec* in the XSpec fitting package: Smith et al. 2001) attenuated by interstellar extinction (*wabs*: Morrison & McCammon 1983). The chemical abundance is fixed to the solar value (Anders & Grevesse 1989). The best-fit parameters are given in table 2 for the amount of extinction (N_H), the plasma temperature ($k_B T$), the X-ray photon flux (f_X), and the absorption-corrected X-ray luminosity (L_X). We obtained a similar but less constrained result for the EPIC spectrum of PS1.

For PS2 and PS3, we used the EPIC data as they are not detected in the XIS image. Source photons were extracted from a 90% encircled energy radius of $\sim 50''$ for both sources (the aperture size is shown at the top right in figure 1b). The background common to both sources was taken from the region shown with the thick dashed circle in figure 1b. A suggestion of a faint Fe K emission line is found for PS2 in the EPIC spectra, but other lines are not seen due to lack of counts (figure 3b and 3c). The PS2 and PS3 spectra were fitted using the same model with PS1. The best-fit parameters are also given in table 2.

3.2.2. Diffuse Sources

We next present the spectra of diffuse sources using XIS. Figure 4 shows their background-subtracted spectra. For DS1, source photons were extracted from a region defined by the emission morphology in the S XV narrow-band image (the thin solid ellipse in figure 2). Spectra of faint diffuse sources are prone to uncertainties stemming from the background subtraction. We considered the following to minimize possible systematic effects. First, the data in the same observation (the north field) were used both for the source and background signals. Second, the back-

³ See (<http://xmm.vilspa.esa.es/sas/>).

⁴ See (<http://xmm.emac.esa.int/docs/documents/CAL-TN-0018.pdf>) for details.

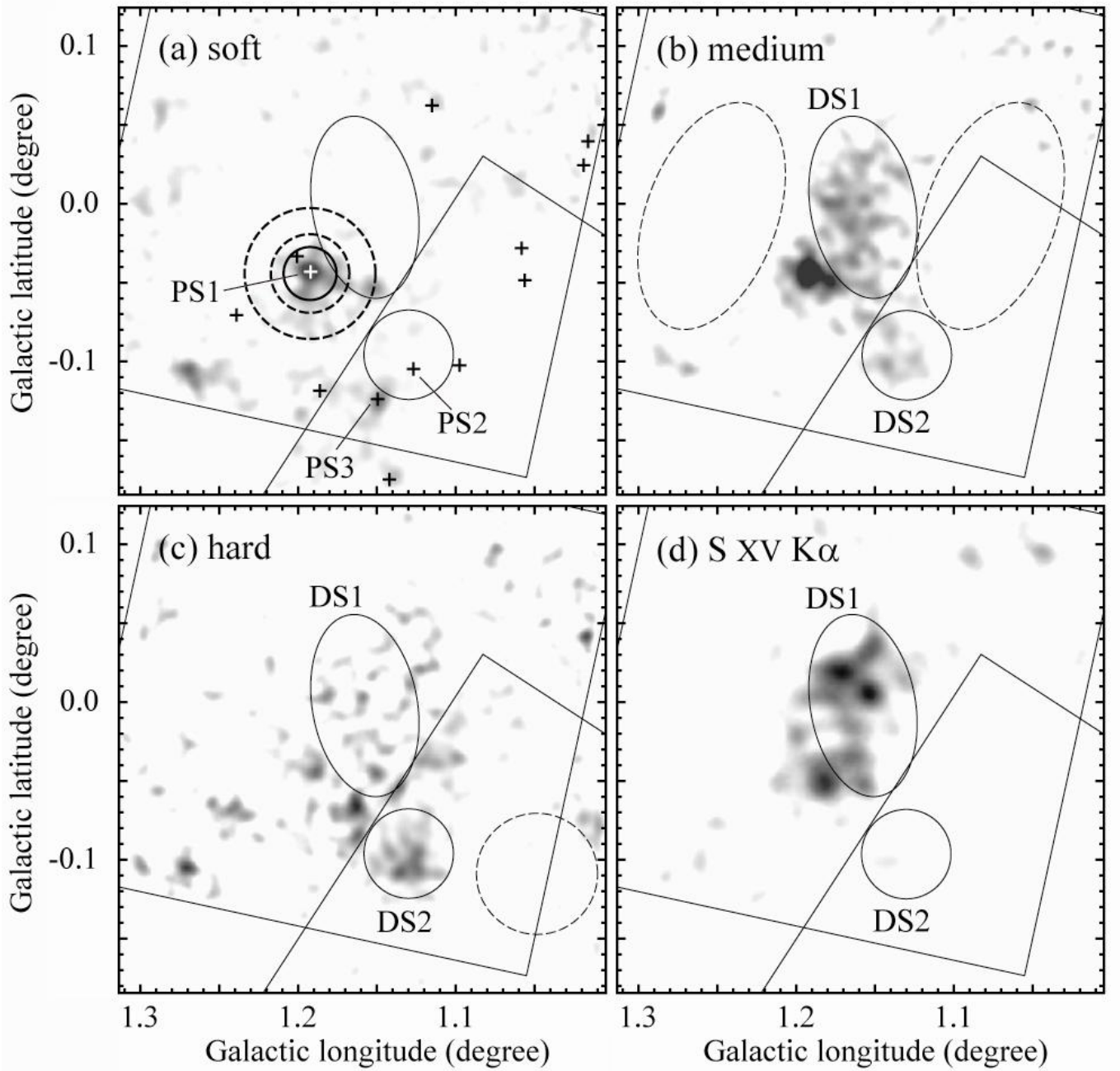


Fig. 2. Close-up XIS images of the Sgr D H II complex in various energy bands: (a) soft (0.7–2.0 keV), (b) medium (2.0–4.0 keV), (c) hard (4.0–5.5 keV), and (d) S XV $K\alpha$ (2.4–2.5 keV). Crosses in (a) represent positions of point sources by XMM-Newton (Watson 2007). The source and background extraction regions are shown with solid and broken symbols, respectively; thick circles for PS1 and thin ellipses for DS1 and DS2. See § 3.2.1 and § 3.2.2 for details. The images were processed in the same way as the wide-band XIS image (figure 1a).

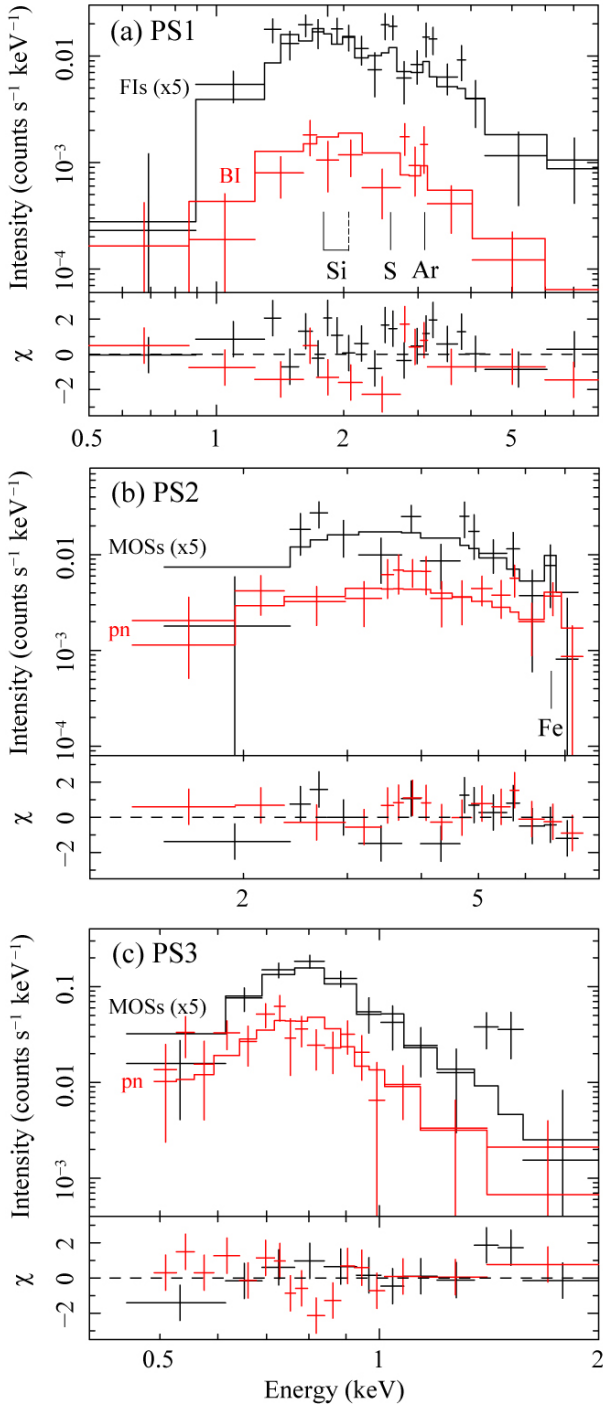


Fig. 3. Background-subtracted spectra (pluses) and the best-fit models (histograms) of PS1–3 (a–c) in the top panels and the residuals to the fit in the bottom panels. For PS1, XIS merged FI and BI spectra are shown in black and red. For PS2 and PS3, EPIC merged MOS and pn spectra are shown in black and red. Black spectra are scaled upward by a factor of 5 for clarity.

Table 2. Best-fit parameters of the point-like sources.

Parameter	PS1	PS2	PS3
Data	XIS	EPIC	EPIC
N_{H} (10^{22} cm $^{-2}$)*	$2.1^{+0.6}_{-0.5}$	$5.7^{+2.0}_{-1.6}$	<0.30
$k_{\text{B}}T$ (keV)*	$1.9^{+0.6}_{-0.4}$	$7.6^{+\infty}_{-7.6}$	$0.48^{+0.08}_{-0.12}$
f_{X} (s $^{-1}$ cm $^{-2}$) †	2.9×10^{-5}	1.7×10^{-5}	1.3×10^{-5}
L_{X} (erg s $^{-1}$) ‡	7.4×10^{32}	2.1×10^{33}	$<2.2 \times 10^{30}$
$\chi^2/\text{d.o.f.}$	46/32	24/27	26/26

* Statistical uncertainty is represented by the 90% confidence intervals.

† Values in the 0.7–8.0 keV band.

‡ The absorption is corrected and the distances are assumed to be 6.8 kpc (PS1), 8.0 kpc (PS2), and <0.97 kpc (PS3). See §4.2 for details.

ground spectrum was constructed from two regions at the same Galactic latitude (the thin dashed ellipses in figure 2b) as the background is dominated by the Galactic center diffuse X-ray emission distributed symmetrically with respect to the Galactic plane (Koyama et al. 1989; Yamauchi et al. 1990). Third, the difference in the effective area due to the different off-axis angles between the source and background regions was taken into account (Hyodo et al. 2008).

For DS2, we used both the north and south field data. The source spectrum was integrated from a ~ 1.7 radius to encompass the Sgr D H II core (the thin solid circle in figure 2). The background subtraction was performed separately in each field and then merged. In the north field, we utilized the background region for DS1, which happens to be at the symmetric position to the Galactic plane with DS2. In the south field, the background was constructed from the thin dashed circle in figure 2c. Other procedures follow DS1.

The spectra of DS1 and DS2 are both characterized by emission lines from highly ionized atoms (figure 4). Thermal fits were tried using the same model with the point sources. Because of stronger signal, we are able to derive the chemical abundances relative to solar for elements with conspicuous emission lines (Z_{S} , Z_{Ar} , Z_{Ca} , and Z_{Fe}). The best-fit values are summarized in table 3. For DS1, we also tried a non-equilibrium ionization model (*nei*; Borkowski et al. 2001). This examines how much a plasma has relaxed toward a collisional equilibrium among ions and electrons. The degree of the relaxation is parameterized by $n_e t$, where n_e is the electron density and t is the time from the plasma creation. A lower limit of $n_e t$ was derived as $\sim 10^{11.2}$ s cm $^{-3}$, which is consistent with DS1 being in collisional equilibrium ($n_e t > 10^{12}$ s cm $^{-3}$; Masai 1984). For DS2, we found that an additional Gaussian model at ~ 6.4 keV improves the fit (F-test significance of $\sim 98\%$) with an equivalent width of ~ 270 eV. More counts are necessary to confirm this.

Because the DS2 emission may largely originate from unresolved point sources, we examined time variation. Light curves in several energy bands are tested against the null hypothesis that the flux is constant using the χ^2

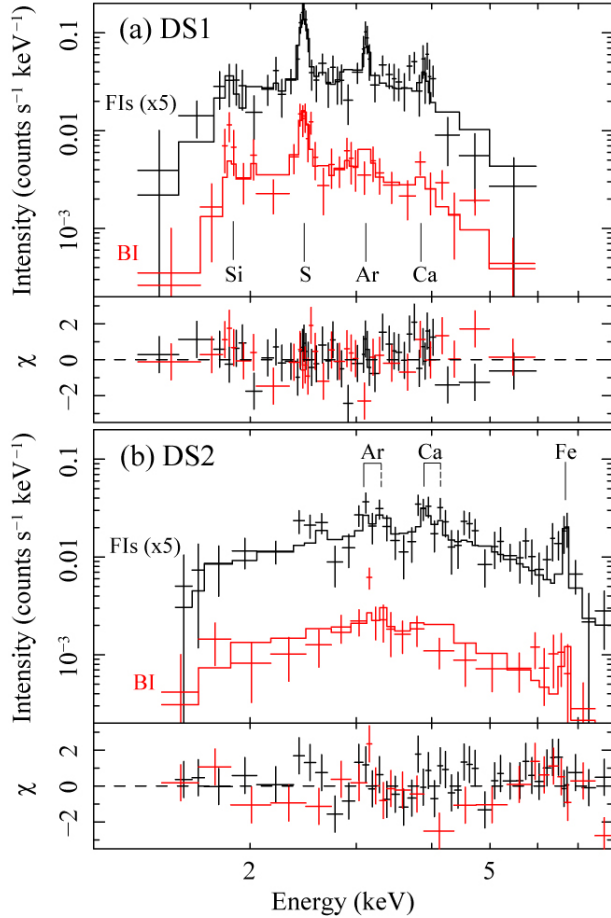


Fig. 4. Background-subtracted XIS spectra and the best-fit models of (a) DS1 and (b) DS2. Symbols follow figure 3.

statistics. We found a marginal variability (significant at a $\sim 97\%$ level) in DS2 in the north field data. For comparison, we conducted the same procedure for DS1 and the background regions. Their signals were found to be constant at high confidence levels. We thus believe that the procedure to test the time variability is reliable, and that DS2 varies.

4. Discussion

4.1. Diffuse Source DS1

4.1.1. Nature of X-ray Emission

We first argue that the level of contamination to DS1 by point sources is negligible. The largest contaminant is PS1 among all point sources listed in the XMM-Newton catalog (pluses in figure 2a), but its contribution accounts only for $\sim 3\%$ of the total XIS counts of DS1. Other point sources make even smaller contributions.

We next argue that DS1 is an extended source. We retrieved optical images using the Digitized Sky Survey from the Space Telescope Science Institute⁵ and near-infrared (NIR) and mid-infrared (MIR) images respectively using the Two Micron All Sky Survey (Skrutskie et al. 1997)

⁵ See (http://archive.stsci.edu/cgi-bin/dss_form) for details.

Table 3. Best-fit parameters of the diffuse sources by XIS.

Parameter	DS1	DS2
N_{H} (10^{22} cm $^{-2}$) [*]	$8.5^{+1.4}_{-1.2}$	$5.6^{+2.3}_{-1.0}$
$k_{\text{B}}T$ (keV) [*]	$0.91^{+0.17}_{-0.17}$	$3.4^{+1.1}_{-1.2}$
Z_{S} (Z_{\odot}) [*]	$1.6^{+0.5}_{-0.4}$	1 (fixed)
Z_{Ar} (Z_{\odot}) ^{*†}	$1.8^{+1.1}_{-0.9}$	$4.8^{+4.0}_{-3.0}$
Z_{Ca} (Z_{\odot}) ^{*†}	$1.8^{+1.1}_{-0.9}$	$4.8^{+4.0}_{-3.0}$
Z_{Fe} (Z_{\odot}) [*]	1 (fixed)	$0.52^{+0.41}_{-0.28}$
f_{X}^{\ddagger} (s $^{-1}$ cm $^{-2}$)	6.9×10^{-5}	4.1×10^{-5}
L_{X}^{\S} (erg s $^{-1}$)	1.4×10^{35}	6.0×10^{33}
$\chi^2/\text{d.o.f.}$	66/75	70/65

^{*} Statistical uncertainty is represented by the 90% confidence intervals.

[†] The values of Z_{Ar} and Z_{Ca} are fixed to one another.

[‡] Values in the 0.7–8.0 keV band.

[§] The absorption is corrected and the distances are assumed to be 8.0 kpc. See § 4.1 and § 4.2 for details.

and the Spitzer Space Telescope (Werner et al. 2004) from the Infrared Science Archive⁶. We compared these images with our X-ray image and found no stellar distribution with a morphology similar to DS1. The point source distribution in the EPIC image (figure 1b) differs significantly from the surface brightness distribution of DS1 in the XIS image (figure 1a). We thus conclude that DS1 is extended in nature, and not an ensemble of unresolved point sources.

The extinction ($\sim 8.5 \times 10^{22}$ cm $^{-2}$) derived from the X-ray spectral fit (table 3) indicates that DS1 is in the GC region (Baganoff et al. 2003). The apparent extent converts to $\sim 9 \times 16$ pc at an 8 kpc distance (Reid 1993). A source like DS1 has not been previously reported in the literature. It is therefore a new celestial object.

4.1.2. Origin of X-ray Emission

Classes of diffuse X-ray emission with an extent of ~ 10 pc include SNRs, irradiated GMCs, pulsar wind nebulae (PWN; Muno et al. 2008), and H II regions (Yusef-Zadeh et al. 2002; Law & Yusef-Zadeh 2004; Wang et al. 2006; Tsujimoto et al. 2007) in the GC region. Since DS1 shows unambiguous thermal features of a ~ 0.9 keV temperature with enhanced abundances of metals, the GMC and PWN origins are unlikely. At the position of DS1, H II regions are not known nor found in our inspection of Spitzer MIR images, which makes an H II region origin also unlikely. The XIS spectrum is akin to those found in SNRs in the GC region (Koyama et al. 2007b; Mori et al. 2008; Nobukawa et al. 2008). Thus, we propose that DS1 is X-ray emission from a new SNR. The lack of X-ray variation is consistent with the SNR interpretation.

SNRs are expected to show nonthermal synchrotron emission in centimeter bands. The Sgr D H II complex has long been considered to have thermal emission, not nonthermal emission, from the flat radio spectral indices (Downes & Maxwell 1966; Swarup et al. 1974; Little 1974; Downes et al. 1979). However, all these results were based on low resolution data, and the spectral indices were dom-

⁶ See (<http://irsa.ipac.caltech.edu/>) for details.

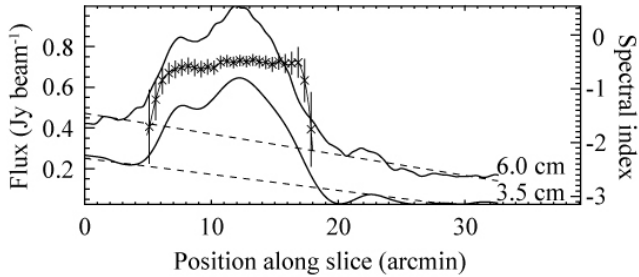


Fig. 5. Profiles of 3.5 cm and 6.0 cm intensity (solid curves) and the spectral index (crosses) between the two bands along the slice shown in figure 6a. Background (dashed lines) is derived by linearly fitting the slope at the two sides of the source region, where the indices are computed. The error bars indicate 1σ uncertainty.

inated by two H II regions with strong thermal emission in and around this complex; the Sgr D H II core and the other H II region to the east (G1.3+0.1 in figure 1a; Mehringer et al. 1998).

The latest work by Law et al. (2008) presented radio continuum maps on spatial scales comparable to the X-ray images. The spectral indices were derived from the 3.5 cm and 6.0 cm continuum maps obtained with GBT along several slices across the Sgr D H II complex. Some indices indicate that there is a mixture of thermal and nonthermal emission.

Using this GBT data set, we constructed the intensity and the spectral index profiles along a slice including DS1 but not the Sgr D H II core (figure 5). The slice was taken from two images (3.5 cm and 6.0 cm) convolved to the same beam size of $\sim 2'.5$. Details of the data and other reduction procedures are described in Law et al. (2008). The background-subtracted index is consistently about -0.5 , indicating that nonthermal synchrotron emission dominates the spectrum (Green 2004). The radio continuum peak corresponds to the position of DS1. This result constitutes independent evidence for classifying DS1 as an SNR.

4.1.3. Structure of the Sgr D H II Complex

We now have sufficient information to decompose and deproject the Sgr D H II complex. The data are displayed in figure 6 with the same scale as figure 1. Figure 6 (a) is composed of the Suzaku X-ray (0.7–5.5 keV; blue), Spitzer MIR (24 μm ; green), and GBT radio continuum (6.0 cm; red) images. In this color code, SNRs appear in magenta with X-ray and nonthermal radio emission such as DS1 and the southwestern part of the Sgr D SNR. H II regions appear in yellow with MIR and thermal radio emission, which include G1.3+0.1 and another H II region inferred by Downes et al. (1979) in the northeast of the Sgr D SNR (we name this component G1.05–0.14). The Sgr D H II core, which has emission in all three bands, does not appear white because the Spitzer image is saturated. Figure 6 (b) is a superposition of the X-ray image with millimeter emission line maps in two different velocities at the local standard of rest; 100 km s^{-1} by CO ($J = 3-2$) in red contours (Oka et al. 2007) taken by the Atacama

Submillimeter Telescope Experiment and -15 km s^{-1} by CS ($J = 1-0$) in blue contours (Tsuboi et al. 1999) taken by the Nobeyama 45 m telescope.

We argue that “tail” is the new SNR (we name G1.2–0.0) and the northwestern part of it is bright in X-ray as DS1. The X-ray morphology of DS1 is not well-correlated with the well-defined shell labeled “extended” in figure 1a. It is therefore unlikely that the two objects are physically related. It is more reasonable to consider that DS1 is associated with “tail”. The index across “tail” is almost constant (figure 5), suggesting that this is a uniform structure. Both X-ray and radio properties indicate that this is an SNR. The X-ray is bright only in the western part of the imperfect shell-like morphology of the “tail”. The lack of X-ray emission in other parts is attributable to an intervening GMC seen in figure 6 (b). The CO emission with a 100 km s^{-1} velocity (red contours) is anticorrelated with the X-ray emission; DS1 is just outside of the sharp boundary of the CO cloud. The extinction along this GMC is $N_{\text{H}} \sim 10^{24} \text{ cm}^{-2}$ from the CO data (private communication with T. Oka), which is sufficient to block the $k_{\text{B}}T \sim 0.9 \text{ keV}$ X-ray emission behind it.

The Sgr D H II core is associated with a GMC in a different velocity (blue contours), which was suggested by Lis (1991) and Liszt (1992). Blum & Damiani (1999) proposed that “core” is a blister H II region on the GMC. We speculate that the H II region G1.05–0.14 is another blister on the other side of the GMC. H 109 α emission is detected at this position and its velocity is the same with the GMC (Pauls & Mezger 1975).

It is now clear that Sgr D H II complex is not a single H II region and its environment as was considered in the past. We propose that an SNR and two H II regions on both sides of a GMC are projected along the same line of sight. The SNR lies behind the H II regions, which is justified by a larger N_{H} value in DS1 (a part of the SNR) than in DS2 (“core”). The SNR position behind the 100 km s^{-1} cloud puts this object in or behind the GC region, whereas the H II regions associated with a GMC at -15 km s^{-1} is on the near side of the GC in agreement with the NIR star count study (Blum & Damiani 1999).

4.2. Other X-ray Sources

4.2.1. Point Sources PS1–PS3

PS1 and PS3 are sources 7 and 11 respectively in the XMM-Newton study by Sidoli et al. (2006). PS1 has several anonymous NIR sources within the positional uncertainty, and its counterpart cannot be identified. PS3 is identified as HD 316290 in Sidoli et al. (2006), which is an F8 star with the B -band and V -band magnitudes of 10.3 mag and 9.8 mag, respectively (Nesterov et al. 1995).

We consider that both sources are foreground objects from their values of N_{H} . Assuming an interstellar hydrogen density of $n_{\text{H}} = 1 \text{ cm}^{-3}$, we derived the distance to PS1 as $\sim 6.8 \text{ kpc}$ and constrained that to PS3 as $\lesssim 0.97 \text{ kpc}$, respectively. The X-ray spectrum and luminosity suggest that both sources are individual stars, but their nature is not constrained any further.

PS2, on the other hand, shows an N_{H} value consistent

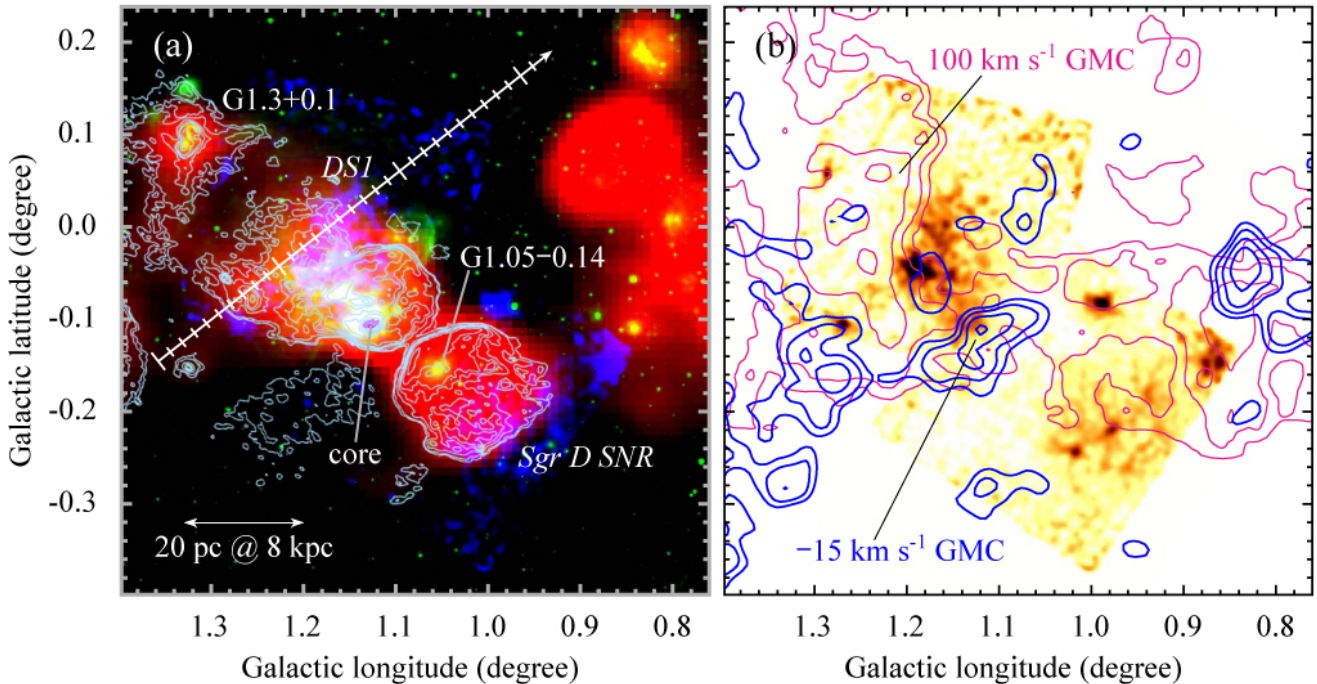


Fig. 6. (a) Composite color image with Suzaku X-ray (0.7–5.5 keV) in blue, Spitzer MIR (24 μm) in green, and GBT radio (6.0 cm) in red. The slice for the radio continuum index (figure 5) is shown with a ticked vector. Objects are labeled in *Italic* for SNRs and in Roman for H II regions. (b) X-ray image with CO ($J = 3-2$) emission at $100 \pm 5 \text{ km s}^{-1}$ (Oka et al. 2007) in red contours and CS ($J = 1-0$) emission at $-15 \pm 5 \text{ km s}^{-1}$ (Tsuboi et al. 1999) in blue contours.

with being in the GC region. We identify a bright NIR source (star A in Blum & Damiani 1999) within the position uncertainty of PS2, which is located $\sim 8''$ north to the center of the Sgr D H II core. The NIR photometry of the star can not distinguish an M giant photosphere with the K -band extinction $A_K = 1.0 \text{ mag}$ or 10,000 K blackbody with $A_K = 2.4 \text{ mag}$ (Blum & Damiani 1999). The X-ray result favors the latter with N_{H} compatible to the larger A_K value.

4.2.2. Diffuse Source DS2

Similarly to DS1, we first evaluate the level of contamination by point sources. Two bright point sources (PS2 and PS3) are found in and around DS2. PS3 has a different X-ray hardness than DS2, and its contribution is minor above 2 keV (figures 3c and 4b). However, the contamination by PS2 is significant. By comparing the time-averaged flux of PS2 by EPIC and DS2 by XIS, $\sim 40\%$ of 0.7–8.0 keV counts of DS2 is attributable to PS2. Similar spectral shapes between PS2 and DS2 (figures 3b and 4b) and the XIS detection of a marginal flux variation during the north field observation indicate that a significant fraction of the DS2 emission stems from PS2.

Nevertheless, PS2 alone cannot account for all properties of DS2. DS2 has an extent inconsistent with a single point source. Figure 7 shows the background-subtracted

radial profile of DS2 around PS2 in comparison to a simulated radial profile of a point-like source. The excess emission is noticeable in the profile as well as in the X-ray image (figure 2c), where the diffuse emission is localized to the northeast of PS2.

The origin of the excess emission is uncertain. It can be either an ensemble of numerous unresolved point sources or the truly extended emission associated with the H II region. Considering a large concentration of stars in the Sgr D H II core (Blum & Damiani 1999; Dutra et al. 2003), the former possibility is likely. If it is of an extended nature, DS2 has quite a hard thermal spectrum for diffuse emission in H II regions, which is comparable to only a few cases (Moffat et al. 2002; Ezoe et al. 2006). The metallicity (table 3) above one solar is larger than diffuse X-ray emission in other H II regions (e.g. Hyodo et al. 2008), which may be due to the enhanced metallicity in the GC region (Cunha et al. 2007). The current data do not give a conclusive interpretation for this emission. Further observations are expected.

5. Summary

We presented a Suzaku X-ray study of the Sgr D H II complex. XIS detected two diffuse X-ray sources and ob-

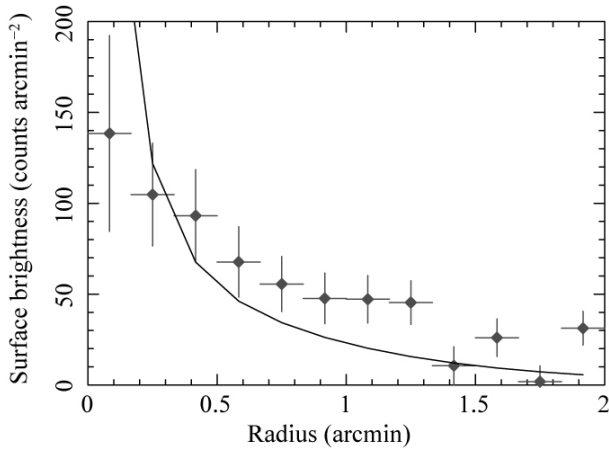


Fig. 7. Radial profile of the background-subtracted intensity around PS2 (solid pluses with dots), which is fitted with a simulated radial profile of a point-like source at the same detector position (solid curve). The energy range of 2.0–5.5 keV is used to suppress the emission by PS3. The observed profile is constructed from the north field data.

tained their high signal-to-noise ratio spectra for the first time. Both sources have a thermal origin with emission lines from highly ionized atoms.

One of the diffuse sources is associated with an H II region and the other is a newly identified source. We use the X-ray characteristics to conclude that the new source is a new SNR in the GC region. The radio continuum data reinforces the idea.

By assembling images across wavelengths, we proposed a new view of the Sgr D H II complex. It is a projection of an SNR in or beyond the GC and a GMC with two blister H II region in front of it. This revises a long-standing view that the Sgr D H II region is a single H II region and its environment.

In this study, we demonstrated the capability of Suzaku XIS to investigate diffuse X-ray emission at low surface brightnesses. Along with the high-resolution radio and infrared images, the Suzaku X-ray data played a critical role in better understanding Sgr D, which is conceivably the case for other regions in the GC as well.

The authors thank Shigeo Yamauchi at Iwate University and Eric D. Feigelson at Pennsylvania State University for improving the draft and Tomoharu Oka at Keio University for providing the CO data. Support for this work was provided by the National Aeronautics and Space Administration (NASA) through Chandra Postdoctoral Fellowship Award Number PF6-70044 issued by the Chandra X-ray Observatory Center, which is operated by the Smithsonian Astrophysical Observatory for and on behalf of the NASA under contract NAS8-03060. Y.H. acknowledges financial support from the Japan Society for the Promotion of Science. This work is supported by a Grants-in-Aid for the 21st Century COE “Center for Diversity and Universality in Physics” and for Scientific Researches on Priority Areas in Japan (Fiscal Year 2002–

2006) “New Development in Black Hole Astronomy” and another (No.18204015) from the Ministry of Education, Culture, Sports, Science and Technology of Japan.

The research has made use of the SIMBAD database, operated at CDS, Strasbourg, France. The Digitized Sky Surveys were produced at the Space Telescope Science Institute under U.S. Government grant NAG W-2166. The images of these surveys are based on photographic data obtained using the Oschin Schmidt Telescope on Palomar Mountain and the UK Schmidt Telescope. The plates were processed into the present compressed digital form with the permission of these institutions. This research has also made use of the NASA/IPAC Infrared Science Archive, which is operated by the Jet Propulsion Laboratory, California Institute of Technology, under contract with the NASA.

References

- Anders, E., & Grevesse, N. 1989, *Geochim. Cosmochim. Acta*, 53, 197
- Arnaud, K. A. 1996, *Astronomical Data Analysis Software and Systems V*, 101, 17
- Baganoff, F. K., et al. 2003, *ApJ*, 591, 891
- Bautz, M. W., Kissel, S. E., Prigozhin, G. Y., LaMarr, B., Burke, B. E., & Gregory, J. A. 2004, *Proc. SPIE*, 5501, 111
- Becker, R. H., Smith, B. W., White, N. E., Holt, S. S., Boldt, E. A., Mushotzky, R. F., & Serlemitsos, P. J. 1979, *ApJ*, 234, L73
- Blum, R. D., & Daminieli, A. 1999, *ApJ*, 512, 237
- Borkowski, K. J., Lyerly, W. J., & Reynolds, S. P. 2001, *ApJ*, 548, 820
- Cunha, K., Sellgren, K., Smith, V. V., Ramirez, S. V., Blum, R. D., & Terndrup, D. M. 2007, *ApJ*, 669, 1011
- Downes, D., & Maxwell, A. 1966, *ApJ*, 146, 653
- Downes, D., Goss, W. M., Schwarz, U. J., & Wouterloot, J. G. A. 1979, *A&AS*, 35, 1
- Dutra, C. M., Ortolani, S., Bica, E., Barbuy, B., Zoccali, M., & Momany, Y. 2003, *A&A*, 408, 127
- Ezoe, Y., Kokubun, M., Makishima, K., Sekimoto, Y., & Matsuzaki, K. 2006, *ApJ*, 638, 860
- Green, D. A. 2004, *Bulletin of the Astronomical Society of India*, 32, 335
- Hyodo, Y., Tsujimoto, M., Hamaguchi, K., Koyama, K., Kitamoto, S., Maeda, Y., Tsuboi, Y., & Ezoe, Y. 2008, *PASJ*, 60, S85
- Ishisaki, Y., et al. 2007, *PASJ*, 59, S113
- Jansen, F., et al. 2001, *A&A*, 365, L1
- Koyama, K., Awaki, H., Kunieda, H., Takano, S., & Tawara, Y. 1989, *Nature*, 339, 603
- Koyama, K., et al. 2007a, *PASJ*, 59, S23
- Koyama, K., et al. 2007b, *PASJ*, 59, S221
- LaRosa, T. N., Kassim, N. E., Lazio, T. J. W., & Hyman, S. D. 2000, *AJ*, 119, 207
- Law, C. J., Yusef-Zadeh, F., Cotton, W. D., & Maddalena, R. J. 2008, *ApJS*, in press
- Law, C., & Yusef-Zadeh, F. 2004, *ApJ*, 611, 858
- Lis, D. C. 1991, *ApJ*, 379, L53
- Liszt, H. S. 1992, *ApJS*, 82, 495
- Little, A. G. 1974, in *IAU Symp. 60, Galactic Radio Astronomy*, ed. F. J. Kerr & S. C. Simonson III (Dordrecht: Reidel), 491

- Masai, K. 1984, *Ap&SS*, 98, 367
- Mehring, D. M., Goss, W. M., Lis, D. C., Palmer, P., & Menten, K. M. 1998, *ApJ*, 493, 274
- Mitsuda, K., et al. 2007, *PASJ*, 59, S1
- Moffat, A. F. J., et al. 2002, *ApJ*, 573, 191
- Mori, H., Tsuru, T. G., Hyodo, Y., Koyama, K., & Senda, A. 2008, *PASJ*, 60, S183
- Morrison, R., & McCammon, D. 1983, *ApJ*, 270, 119
- Muno, M. P., Baganoff, F. K., Brandt, W. N., Morris, M. R., & Starck, J.-L. 2008, *ApJ*, 673, 251
- Murakami, H., Koyama, K., Sakano, M., Tsujimoto, M., & Maeda, Y. 2000, *ApJ*, 534, 283
- Nesterov, V. V., Kuzmin, A. V., Ashimbaeva, N. T., Volchkov, A. A., Röser, S., & Bastian, U. 1995, *A&AS*, 110, 367
- Nobukawa, M., et al. 2008, *PASJ*, 60, S191
- Odenwald, S. F., & Fazio, G. G. 1984, *ApJ*, 283, 601
- Oka, T., Nagai, M., Kamegai, K., Tanaka, K., & Kuboi, N. 2007, *PASJ*, 59, 15
- Pauls, T., & Mezger, P. G. 1975, *A&A*, 44, 259
- Reid, M. J. 1993, *ARA&A*, 31, 345
- Sakano, M., Koyama, K., Murakami, H., Maeda, Y., & Yamauchi, S. 2002, *ApJS*, 138, 19
- Serlemitsos, P. J., et al. 2007, *PASJ*, 59, S9
- Sidoli, L., Mereghetti, S., Treves, A., Parmar, A. N., Turolla, R., & Favata, F. 2001, *A&A*, 372, 651
- Sidoli, L., Mereghetti, S., Favata, F., Oosterbroek, T., & Parmar, A. N. 2006, *A&A*, 456, 287
- Skrutskie, M. F., et al. 1997, *The Impact of Large Scale Near-IR Sky Surveys*, 210, 25
- Smith, R. K., Brickhouse, N. S., Liedahl, D. A., & Raymond, J. C. 2001, *ApJ*, 556, L91
- Strüder, L., et al. 2001, *A&A*, 365, L18
- Swarup, G., Gopal-Krishna, & Sarma, N. V. G. 1974, *Galactic Radio Astronomy*, 60, 499
- Tawa, N., et al. 2008, *PASJ*, 60, S11
- Townsley, L. K., Feigelson, E. D., Montmerle, T., Broos, P. S., Chu, Y.-H., & Garmire, G. P. 2003, *ApJ*, 593, 874
- Tsuboi, M., Handa, T., & Ukita, N. 1999, *ApJS*, 120, 1
- Tsujimoto, M., Hyodo, Y., & Koyama, K. 2007, *PASJ*, 59, S229
- Turner, M. J. L., et al. 2001, *A&A*, 365, L27
- Uchiyama, H., et al. 2007, *Proc. SPIE*, 6686, 66860P
- Uchiyama, Y., et al. 2008, *PASJ*, 60, S35
- Werner, M. W., et al. 2004, *ApJS*, 154, 1
- Wang, Q. D., Dong, H., & Lang, C. 2006, *MNRAS*, 371, 38
- Watson, M. 2007, *Astronomy and Geophysics*, 48, 30
- Wolk, S. J., Bourke, T. L., Smith, R. K., Spitzbart, B., & Alves, J. 2002, *ApJ*, 580, L161
- Yamauchi, S., Kawada, M., Koyama, K., Kunieda, H., & Tawara, Y. 1990, *ApJ*, 365, 532
- Yusef-Zadeh, F., Law, C., Wardle, M., Wang, Q. D., Fruscione, A., Lang, C. C., & Cotera, A. 2002, *ApJ*, 570, 665
- Yusef-Zadeh, F., Hewitt, J. W., & Cotton, W. 2004, *ApJS*, 155, 421